

The red blazar PMN J2345–1555 becomes blue

G. Ghisellini^{*}, F. Tavecchio, L. Foschini, G. Bonnoli, G. Tagliaferri

¹ INAF – Osservatorio Astronomico di Brera, Via Bianchi 46, I–23807 Merate, Italy

8 March 2022

ABSTRACT

The Flat Spectrum Radio Quasar PMN J2345–1555 is a bright γ -ray source, that recently underwent a flaring episode in the IR, UV and γ -ray bands. The flux changed quasi simultaneously at different frequencies, suggesting that it was produced by a single population of emitting particles, hence by a single and well localized region of the jet. While the overall Spectral Energy Distribution (SED) before the flare was typical of powerful blazars (namely two broad humps peaking in the far IR and below 100 MeV bands, respectively), during the flare the peaks moved to the optical–UV and to energies larger than 1 GeV, to resemble low power BL Lac objects, even if the observed bolometric luminosity increased by more than one order of magnitude. We interpret this behavior as due to a change of the location of the emission region in the jet, from within the broad line region, to just outside. The corresponding decrease of the radiation energy density as seen in the comoving frame of the jet allowed the relativistic electrons to be accelerated to higher energies, and thus produce a “bluer” SED.

Key words: BL Lacertae objects: general — quasars: general — radiation mechanisms: non-thermal — gamma-rays: theory — X-rays: general

1 INTRODUCTION

PMN J2345–1555 is a Flat Radio Spectrum Quasar (FSRQ) at $z = 0.621$ (Healey et al. 2008), bright in γ -rays, and detected by the Large Area Telescope (LAT) onboard the *Fermi* satellite in the first 3 months of its operation (Abdo et al. 2009), and later present in the 1LAC (catalog of AGN detected in the first 11 months of operations, Abdo et al. 2010) and 2LAC (first 2 years, Nolan et al. 2012). The γ -ray spectra were described by simple power laws. The fluxes above 100 MeV are reported in Tab. 1, together with the photon spectral indices. It can be seen that the source varied on long timescales, even if the reported fluxes are averaged over the entire period of observations. On the other hand the spectral index Γ was always greater than 2, indicating a νF_ν peak at energies smaller than 100 MeV. This is typical for the FSRQ class (see Abdo et al. 2010; Ghisellini, Maraschi & Tavecchio 2009).

At the beginning of 2013 the source underwent a major flare, reaching, on Jan 13, 2013, a flux above 100 MeV of $(110 \pm 20) \times 10^{-8}$ ph cm⁻² s⁻¹, more than 15 times the average photon flux listed in the 2LAC catalog (Tanaka 2013). Most interestingly, as noted in the telegram by Tanaka (2013), the spectral index became harder, $\Gamma = 1.78 \pm 0.13$. This implies a rising spectrum in νF_ν , which is instead typical of low power blazars, namely high energy peaked BL Lac objects. Since the spectrum hardened, the luminosity variation between Jan 13 2013 and the average value in the 2LAC catalog was almost a factor 30. The spectral change was accompanied by a flaring behavior not only in γ -rays, but also in IR,

Catalog/Date	F_{-8} [>0.1 GeV]	Γ_{LAT}	$\log L_\gamma$
LBAS	10.3 ± 1.3	2.42 ± 0.12	46.89
1LAC	3.5	2.37 ± 0.10	46.44
2LAC	6.5	2.19 ± 0.04	46.79
Jan 13 2013	110 ± 20	1.78 ± 0.13	48.25

Table 1. Fluxes F_{-8} in units of 10^{-8} ph cm⁻² s⁻¹ above 100 MeV and corresponding spectral indices as reported in different catalogs, and in Tanaka et al. (2013) for the Jan 13, 2013 data. The last column reports the K-corrected [0.1–100 GeV] luminosities.

optical and UV (Carrasco et al. 2013; Donato et al. 2013), where the source increased its flux by almost 2 orders of magnitude, and in X-rays (Donato et al. 2013), albeit with a more modest increase.

Although other FSRQs with a relatively hard γ -ray spectrum have been already detected by *Fermi* (discussed in Padovani, Giommi & Rau 2012 and Ghisellini et al. 2012), it is the first time that we can well document, in a given FSRQ (i.e. a blazar with relatively strong broad emission lines), the change from a soft ($\Gamma_{\text{LAT}} > 2$) to a hard ($\Gamma_{\text{LAT}} < 2$) γ -ray slope, accompanied by an intense flare of the source from the near IR to the γ -ray band. Previous hardening of the γ -ray spectrum have been observed in the FSRQ 4C +21.35 (=1222+216, Tanaka et al. 2011, interpreted by Foschini et al. 2011 as a change in the location of the dissipation region in the same source) and in BL Lac (Bloom et al. 1997).

The aim of this letter is to analyze the available data concerning the flare, to compare them to the existing older observations,

* Email: gabriele.ghisellini@brera.inaf.it

and to construct a coherent picture of what caused the “red to blue” transition of this blazar.

We use a cosmology with $h = \Omega_{\Lambda} = 0.7$ and $\Omega_M = 0.3$.

2 DATA ANALYSIS

2.1 *Swift* observations

Swift XRT and UVOT data were analyzed by using the `HEASOFT` v. 6.13 software package with the `CALDB` updated on 21 January 2013. XRT data were processed with `xrtpipeline` v. 0.12.6 with standard parameters. The extracted count spectra have been grouped to have at least 25 counts per bin, in order to adopt the χ^2 test and analyzed with `xspec` v. 12.8.0 in the 0.3–10 keV energy band. The basic adopted model was a redshifted power law with a fixed Galactic absorption column of $N_H = 1.64 \times 10^{20} \text{ cm}^{-2}$ (Kalberla et al. 2005). However, in the 2013 Jan 14 observation (obsID 00038401009) a broken power law model is required at 99.53% according to the *ftest*. See Tab. 2.

Optical/UV photometry was done with UVOT, by adopting a $5''$ -sized region for the source and a $7''$ – $60''$ source-free annulus for the background. UVOT tasks `uvotimsum` and `uvotsource` were used to perform the analysis. The observed magnitudes, reported in Tab. 2, were then corrected for the Galactic absorption according to the filter-specific formulas of Cardelli et al. (1989) and converted into physical units flux by using the calibration of Poole et al. (2008) and Breeveld et al. (2010).

2.2 *Fermi*/LAT observations

Publicly available *Fermi* LAT data were retrieved from the Fermi Science Support Center (FSSC) and analyzed by means of the LAT Science Tools v. 9.27.1, together with the Instrument Response Function (IRF) Pass 7 and the corresponding isotropic and Galactic diffuse background models. Source (class 2) photons in the 0.1–100 GeV energy range, collected on January 11–14 and coming from direction within 10° from the nominal source position were selected and filtered through standard quality cuts. Standard analysis steps compliant with the FSSC recommendations were then performed. Besides the target and backgrounds, all the 2FGL point sources in the field were included in the model. PMNJ2345–1555 was detected with high statistical significance ($TS = 340$, Mattox et al. 1996) and a high flux [$F_{0.1-100 \text{ GeV}} = (8.76 \pm 0.16) \times 10^{-7} \text{ photons cm}^{-2} \text{ s}^{-1}$] and a flat photon index $\Gamma = -2.02 \pm 0.01$. A significant spectral break at $E_b = 2 \pm 0.5 \text{ GeV}$ is found fitting the data with a broken power law model, with low and high spectral indices $\Gamma_1 = 1.84 \pm 0.15$ and $\Gamma_2 = 2.58 \pm 0.34$. A similar analysis, but made in logarithmically spaced energy bins, gives results consistent with this break (solid black points in Fig. 1). This suggests that the high energy hump in the SED peaks at $\sim 2 \text{ GeV}$.

3 SPECTRAL ENERGY DISTRIBUTION AND MODEL

Fig. 1 shows the SED of the source, and highlights the dramatic flux variations occurred from the IR to the γ -ray bands. The cyan bow-tie corresponds to the maximum seen by *Fermi* on Jan 13, 2013; black symbols correspond to quasi simultaneous data taken between 11 and 14 Jan (*Fermi*), Jan 14 (X-rays and optical–UV by *Swift*). The brown symbols refer to Jan 17, 2013. The red symbols refer to two *Swift* observations merged together taken on Dec. 23,

	23/12/2008 ^a	14/01/2013	17/01/2013
Γ_{single}	1.6 ± 0.4	...	1.9 ± 0.2
Γ_{soft}	...	2.6 ± 0.3	...
Γ_{hard}	...	$1.0_{-0.7}^{+0.5}$...
$E_{\text{break}} \text{ (keV)}$...	$1.7_{-0.4}^{+0.7}$...
χ^2/dof	0.3/1	3.4/6	2.86/8
$F_{0.2-10}$	0.39 ± 0.05	4.6	2.6
<i>V</i>	18.50 ± 0.10	13.93 ± 0.03	14.23 ± 0.03
<i>B</i>	18.61 ± 0.06	14.28 ± 0.03	14.59 ± 0.03
<i>U</i>	17.91 ± 0.05	13.40 ± 0.03	13.71 ± 0.03
<i>W1</i>	17.57 ± 0.07	13.39 ± 0.04	13.71 ± 0.04
<i>M2</i>	17.66 ± 0.05	13.32 ± 0.04	13.71 ± 0.04
<i>W2</i>	17.78 ± 0.04	13.49 ± 0.04	13.88 ± 0.04

Table 2. Top: Results of the X-ray analysis. For all spectra a fixed Galactic $N_H = 1.64 \times 10^{20} \text{ cm}^{-2}$ was assumed. The flux $F_{0.2-10}$ is the unabsorbed flux in the [0.2–10 keV] band in units of $10^{-12} \text{ erg cm}^{-2} \text{ s}^{-1}$. Bottom: UVOT Observed magnitudes. *a*: Average of 2 observations on 23/12/2008 and 10/01/2009.

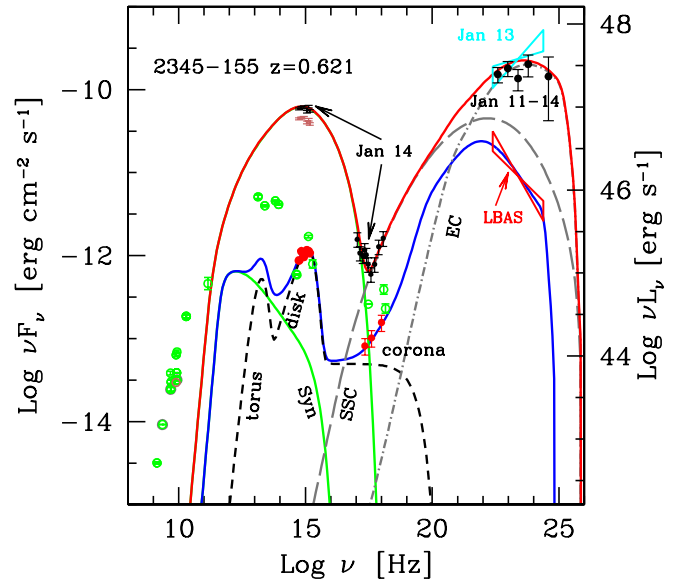


Figure 1. The SED of PMN J2345–1555 and the fitting models. Black points correspond to *Swift*/UVOT and XRT data taken on Jan. 14, 2013 and to *Fermi* data integrating the flux between Jan 11 and 14. The brown points are the UVOT data taken on Jan 17, 2013. The cyan bow-tie corresponds to the maximum seen by *Fermi* on Jan 13, 2013. We can compare the high state of Jan 2013 with the low state observed in Dec 23, 2008 by *Swift* (red points), while the red bow-tie refer to the average state of the first 3 months of *Fermi* operations (LBAS). Green symbols refer to archival data. We show the models for the two states, as explained in the text and with parameters listed in Tab. 3, with the different components labeled.

2008 and Jan 10, 2009. The red bow tie in γ -rays is the average spectrum observed in the first 3 months of operations of *Fermi*.

One of the most interesting features of this SED concerns the X-ray spectrum: being a broken power law, it is strongly suggesting that in this band we see the end of the steep synchrotron component and the emergence of (presumably) the flat inverse Compton (IC) contribution. This is a defining property (Padovani & Giommi 1995) of intermediate BL Lacs (see Tagliaferri et al. 2000 for a similar spectrum in the BL Lac source ON 231). Since in the previ-

ous *Swift*/XRT observation the entire X–ray spectrum was flat, and could be interpreted as IC, we must conclude that the peak of the synchrotron flux shifted towards higher frequencies. As a result, also the IC bump is “bluer”, making the *Fermi*/LAT spectrum flat, and peaking at $h\nu_C \sim 2$ GeV. At the same time, the UVOT data are consistent with a synchrotron peak at $\nu_S \sim 10^{15}$ Hz.

If the IC process with seed photons of frequency ν_{ext} produced externally dominates (External Compton, EC for short), we have (see Tavecchio & Ghisellini 2008):

$$\nu_C \sim \frac{4}{3} \gamma_{\text{peak}}^2 \nu_{\text{ext}} \frac{2\Gamma\delta}{1+z} \rightarrow \gamma_{\text{peak}} \sim \left[\frac{3(1+z)\nu_C}{8\Gamma\delta\nu_{\text{ext}}} \right]^{1/2} \quad (1)$$

where Γ is the bulk Lorentz factor; $\delta = 1/[\Gamma(1 - \beta \cos \theta_v)]$; θ_v is the viewing angle and $\gamma_{\text{peak}} m_e c^2$ is the energy of the electrons emitting at the peaks of the SED. Setting $\nu_C = 4.8 \times 10^{23}$ Hz (i.e. 2 GeV) and $\Gamma = \delta$, we derive $\gamma_{\text{peak}} \sim 700(\Gamma/15)$ or $7000(\Gamma/15)$ according if ν_{ext} is the Hydrogen Ly α or the peak of the IR emission produced by the torus, assumed to be at 3×10^{13} Hz. The synchrotron peak frequency $\nu_S \sim 10^{15}$ Hz then yields:

$$\nu_S = 3.6 \times 10^6 \frac{\gamma_{\text{peak}}^2 B \delta}{1+z} \text{ Hz} \rightarrow B \sim \frac{8\Gamma\nu_{\text{ext}}\nu_S}{1.1 \times 10^7 \nu_C} \text{ G} \quad (2)$$

This gives $B \sim 70(\Gamma/15)$ or $0.7(\Gamma/15)$ G if the seed photons are coming from the broad line region (BLR) or from the IR torus, respectively. The very same relations hold for the SED observed when the γ -ray spectrum is steep, but with different ν_S and ν_C . As we shall see, a coherent scenario explains the large shift in peak frequencies as due to the dissipation region, usually located within the BLR, moving beyond it. In such a case the reduced cooling allowed the electrons to reach larger γ_{peak} , corresponding to larger ν_S and ν_C . We then apply a model along these lines.

3.1 The model

We use the model described in detail in Ghisellini & Tavecchio (2009), and used in our previous blazar studies. For self consistency, and to explain the main parameters listed in Tab. 3, we repeat here the main properties of the model.

The model accounts for several contributions to the radiation energy density, and how these and the magnetic one scale with the distance R_{diss} from the black hole of mass M . We consider radiation from the disk (i.e. Dermer & Schlickeiser 1993), the BLR (e.g. Sikora, Begelman & Rees 1994), a dusty torus (see Błazejowski et al. 2000; Sikora et al. 2002), the host galaxy light and the cosmic background radiation. It is a one–zone, leptonic model.

The emitting region is spherical, of size $R \sim 0.1R_{\text{diss}}$. The jet accelerates in its inner parts with $\Gamma \propto R_{\text{diss}}^{1/2}$ up to a value Γ_{max} .

The electron injection function $Q(\gamma)$ [$\text{cm}^{-3} \text{s}^{-1}$] is assumed to be a smoothly joining broken power–law, with a slope $Q(\gamma) \propto \gamma^{-s_1}$ and γ^{-s_2} below and above a break energy γ_b : The total power injected into the source in relativistic electrons is $P'_i = m_e c^2 V \int Q(\gamma) \gamma d\gamma$, where $V = (4\pi/3)R^3$.

The BLR, reprocessing 10% of the disk luminosity L_d , is assumed to be a thin spherical shell located at a distance $R_{\text{BLR}} = 10^{17} L_{d,45}^{1/2}$ cm. The radiation energy density of the broad lines is constant within the BLR, but it is seen amplified by $\sim \Gamma^2$ by the moving blob (as long as $R_{\text{diss}} < R_{\text{BLR}}$). For illustration, Fig. 3 shows also the case of a “ring–like” BLR, lying in the disk, shaped as a torus of radius R_{BLR} and cross sectional radius equal to $0.1R_{\text{BLR}}$. The U'_{BLR} profile is somewhat smoother in this case. The two cases (spherical and ring–like) should bracket the

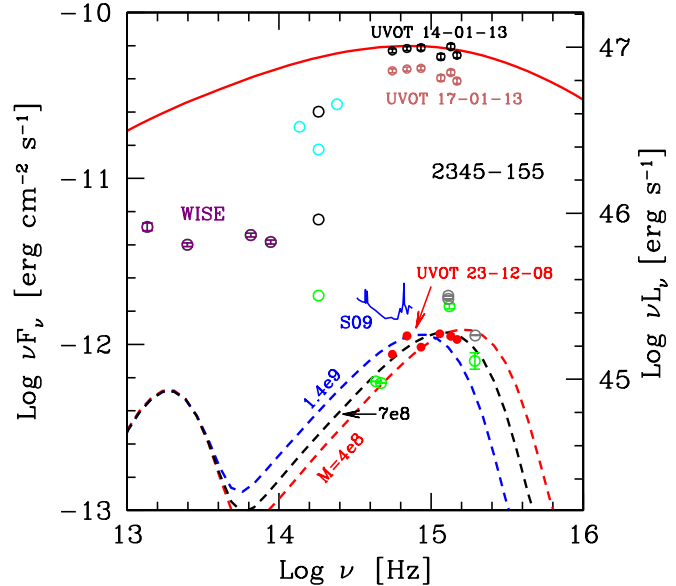


Figure 2. Zoom of the SED of PMN J2345–1555 to better show the IR–UV part of the spectrum. The *Swift*/UVOT data of Dec. 23, 2008 can be described by a standard accretion disk model. Note the upturn in the optical spectrum taken by Shaw et al. (2009), labeled S09. To illustrate the possible uncertainties on the black hole mass, we show three accretion disk (+torus) models that have the same disk luminosity but different black hole masses, as labelled. In Jan 13, 2013 the optical–UV synchrotron flux increased by almost 2 orders of magnitude, largely overtaking the thermal emission.

possible geometrical possibilities. A dusty torus, located at a distance $R_{\text{IR}} = 2.5 \times 10^{18} L_{d,45}^{1/2}$ cm, reprocesses $\sim 30\%$ of L_d in the far IR. In the inner parts of the accretion disk there is an X–ray emitting corona of luminosity $L_X \sim 0.3L_d$ with a spectrum $F(\nu) \propto \nu^{-1} \exp(-h\nu/150 \text{ keV})$.

The energy densities of all these external components are calculated in the jet comoving frame, and used to calculate the resulting EC spectrum. The internally produced synchrotron emission is used to calculate the synchrotron self Compton (SSC) flux.

We adopt a standard Shakura & Sunjaev (1973) accretion disk spectrum. It depends on the black hole mass M and the accretion rate \dot{M} , that can be found if the SED shows signs of disk emission. In this case the total disk luminosity L_d fixes \dot{M} , and the peak frequency of the disk spectrum fixes M . Furthermore, we are helped by the presence of broad lines, that can be used as a proxy for L_d . This method, detailed in Calderone et al. (2013), returns very accurate black hole masses if the peak of the disk emission is visible.

4 RESULTS

Fig. 1 shows the result of the modeling: the red solid curve is the model for the data of Jan 13, 2013, and the solid blue line is the model fitting the Dec. 2008 UVOT and XRT data, together with the average γ -ray flux of the first 3 months of *Fermi*. Both models share the same black hole mass, accretion rate and viewing angle. All used parameters are listed in Tab. 3 that also reports, for ease of the reader, the set of parameters used in Ghisellini et al. (2009), that considered a slightly smaller black hole mass. Fig. 1 shows also the torus, disk and corona emission (unchanged for both states), the synchrotron component and the SSC and EC contributions for the Jan 13 SED. Particularly important is the UVOT spectrum in

Date	R_{diss}	$R_{\text{diss}}/R_{\text{S}}$	M	R_{BLR}	P'_i	L_{d}	$L_{\text{d}}/L_{\text{Edd}}$	B	Γ	θ_{v}	γ_{b}	γ_{max}	ν_{S}	s_1	s_2
[1]	[2]	[3]	[4]	[5]	[6]	[7]	[8]	[9]	[10]	[11]	[12]	[13]	[14]	[15]	[16]
23/12/2008 ^a	132	1100	4e8	190	3.5e-3	3.6	0.06	1.8	13	3	100	4e3	1.e12	-1	2.8
23/12/2008	126	600	7e8	186	1.6e-3	3.5	0.033	1.9	13	2.4	180	5e3	2.7e12	0.2	2.9
13/01/2013	336	1600	7e8	186	0.014	3.5	0.033	0.57	16	2.4	7e3	5e4	1.4e15	0	3.2

Table 3. Parameters of the models shown in Fig. 1 and Fig. 2. *a*: set of parameters used in Ghisellini et al. (2010), where a slightly smaller M was adopted. Col. [1]: date; Col. [2], [3]: dissipation radius in units of 10^{15} cm and in units of R_{S} ; Col. [4]: black hole mass in solar masses; Col. [5]: size of the BLR in units of 10^{15} cm; Col. [6]: power injected in the blob calculated in the comoving frame, in units of 10^{45} erg s^{-1} ; Col. [7], [8]: accretion disk luminosity in units of 10^{45} erg s^{-1} and in units of L_{Edd} ; Col. [9]: magnetic field in Gauss; Col. [10]: bulk Lorentz factor at R_{diss} ; Col. [11]: viewing angle in degrees; Col. [12], [13]: break and maximum random Lorentz factors of the injected electrons; Col. [14]: peak synchrotron frequency ν_{S} (Hz, rest frame); Col. [15] and [16]: slopes of the injected electron distribution [$Q(\gamma)$].

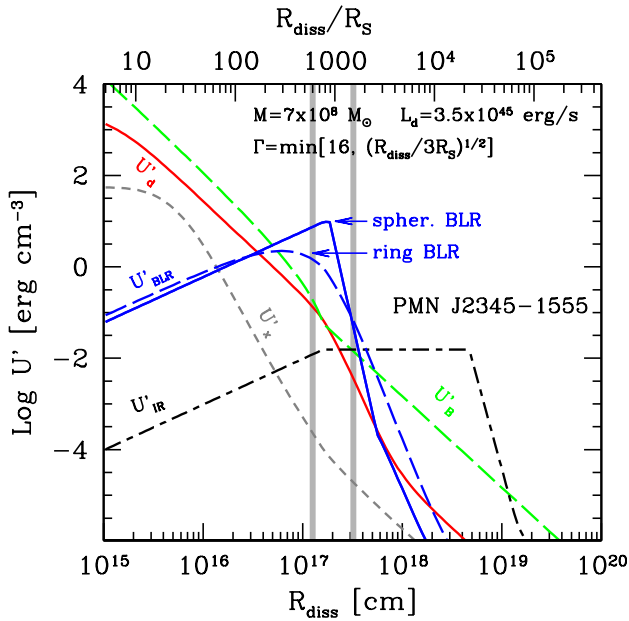


Figure 3. The energy density measured in the comoving frame of the blob as a function of the distance from the black hole, R_{diss} . We show separately the contribution of the magnetic field (U_B), of the radiation coming directly from the disk (U'_d), and its X-ray corona (U'_X), of the radiation produced by the BLR (U'_{BLR}) and by the torus (U'_{IR}). The two vertical grey lines mark the values R_{diss} for the two states of the source. The Jan 13, 2013 flare corresponds to dissipation occurring just beyond the BLR. For illustration, we also show U'_{BLR} for a “ring-like” BLR lying in the disk, shaped as a torus of radius R_{BLR} and cross sectional radius $R_{\text{BLR}}/10$.

Dec 2008, that can be interpreted as the peak of the accretion disk component. The Shaw et al. (2009) optical spectrum is visible in Fig. 2. Its flux is larger than in Dec. 2009, there is a contamination from the synchrotron component at low frequencies, an upturn at large frequencies and the broad MgII and H β lines are well visible. Their luminosities can be used to reconstruct the luminosity of the entire BLR (using the template of Francis et al. 1991 or Vander Berk et al. 2001) and then L_{d} . It agrees with the ones we have adopted, i.e. $L_{\text{d}} \sim 3.5 \times 10^{45}$ erg s^{-1} . Since the UVOT points show a peak in νF_{ν} , we find $M = 7 \times 10^8 M_{\odot}$. To show how well the black hole mass can be determined, we have plotted in Fig. 2 other two disk spectra, of the same L_{d} but with different masses (i.e. 0.4 and 1.4 billion solar masses). With these values the data are not well reproduced. By applying the virial method, Shaw et al. (2009) estimated $M \sim (3 - 6) \times 10^8 M_{\odot}$, using the H β and the

Date	$\log P_r$	$\log P_B$	$\log P_e$	$\log P_p$
23/12/2008 ^a	44.72	44.56	43.97	45.92
23/12/2008	44.39	44.55	43.61	45.62
13/01/2013	45.53	44.54	44.67	45.25

Table 4. Jet power in the form of radiation, Poynting flux, bulk motion of emitting (therefore relativistic) electrons and cold protons, assuming one proton per emitting electron. *a*: set of powers derived in Ghisellini et al. (2010), where a slightly smaller black hole mass was adopted.

MgII lines. Given the uncertainties, these values are well consistent with ours.

To reproduce the two states of the source, we have chosen to modify a minimum numbers of parameters. Besides M and \dot{M} , the models share the same magnetic field profile (i.e. the same Poynting flux $L_B \equiv R^2 \Gamma^2 B^2 c/8$; see Tab. 4). The main changes concern the typical energies of the injected electrons, higher in the high states, the value of R_{diss} and the injected power. We have furthermore assumed that in the high state the bulk Lorentz factor is somewhat larger ($\Gamma=16$ vs. 13). As shown in Fig. 3, all these changes are consistent with the idea that the two states correspond to a different R_{diss} : for the “low” state, $R_{\text{diss}} < R_{\text{BLR}}$, the radiative cooling is strong, electrons cannot reach high energies and the overall SED is “red”. By moving from 600 to 1600 Schwarzschild radii, the radiation energy density drops, letting the electrons to reach higher energies. The magnetic field also decreases [$B \propto (R_{\text{diss}} \Gamma)^{-1}$], but the change of the radiation energy density is more drastic, making the Compton dominance (ratio of the inverse Compton to synchrotron luminosities) to decrease in the high state.

5 DISCUSSION

Fig. 4 shows γ_{peak} as a function of the total radiation energy density (magnetic plus radiative) as seen in the comoving frame of the source. The random Lorentz factor γ_{peak} corresponds to the energy of the electrons emitting most of power (both in synchrotron and in inverse Compton). The grey points are the values of blazars analyzed by us in the past (see Ghisellini et al. 2012 and references therein), while the red squares corresponds to the 4 “blue” blazars discovered by Padovani, Giommi & Rau (2012). As these authors suggested, they are very likely FSRQs with a very powerful optical synchrotron emission, that hides the emission lines. They should therefore correspond to the high state of PMN J2345–1555. The monitoring of these 4 blazars is too sparse to know if they are permanently “in the high state”, or if we caught them by

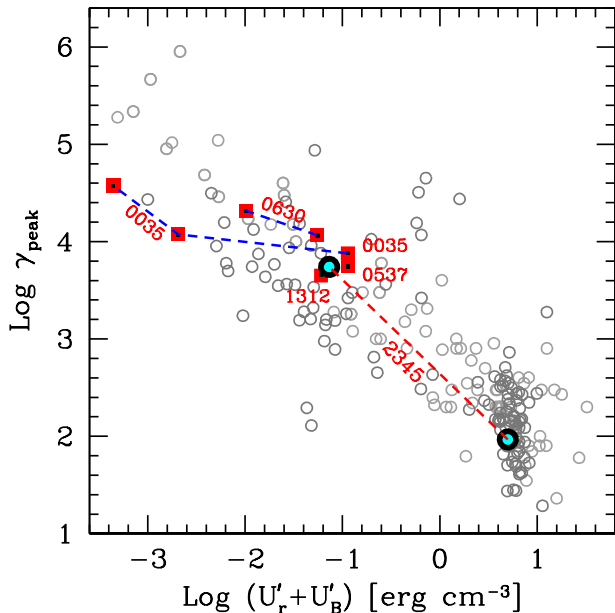


Figure 4. Random Lorentz factor (γ_{peak}) of the electrons emitting at the SED peaks as a function of the total energy density $U' = U'_r + U'_B$ as measured in the comoving frame. Small γ_{peak} and large U' correspond to “red” blazars, while large γ_{peak} and small U' correspond to “blue” blazars. The grey points correspond to blazar analyzed by us in the past (Ghisellini et al., 2012 and references therein), while red symbols refer to the 4 “blue” quasars studied in Padovani, Giommi & Rau (2012) and Ghisellini et al. (2012). PMN J2345–1555 is the first clear example of a blazar shifting from red to blue.

chance. In any case, PMN J2345–1555 demonstrates that a single source can indeed vary not only its overall flux by orders of magnitudes, but also its overall “look” and “color”. In our scheme this is simply due to the change of the location of the dissipation region by a factor less than 3 (from 600 to 1600 Schwarzschild radii in this case). This is sufficient to shift a blazar, in Fig. 4, from the red ($\gamma_{\text{peak}} \lesssim 10^3$ and $U' \gtrsim 0.3$) to the blue zone ($\gamma_{\text{peak}} \gtrsim 10^3$ and $U' \lesssim 0.3 \text{ erg cm}^{-3}$). The top left region of the plane is populated mainly by low power, high energy peaked BL Lacs, lacking strong broad emission lines. For them, we do not expect strong variations of the cooling process when R_{diss} changes (since there is no BLR). Variations are however possible due to changes in the acceleration process, in turn linked to the total power. Larger injected powers (and thus larger observed luminosities) could be associated to larger γ_{peak} , as observed in Mkn 501 (Pian et al. 1998; Tavecchio et al. 2001).

The fact that PMN J2345–1555 is the first FSRQ “caught in the act” suggests that it is a rare phenomenon. Furthermore, out of a sample of hundreds of FSRQs detected by *Fermi*, only 4 were found to be blue by Padovani et al. (2012). This leads us to conclude that only a few per cent of FSRQs dissipate most of their energy beyond the BLR, either occasionally or permanently. In turn, this suggests that the region where the jet dissipates the most is indeed well confined at $R_{\text{diss}} \lesssim 10^3 R_S$. Larger radii (even by a small amount), corresponding to a blue FSRQ, are rare, although not impossible.

We envisage two possibilities to have a dissipation always well localized. The first is internal shocks: two shells initially separated by ΔR and moving with different Γ will collide at $R_{\text{diss}} \sim \Gamma^2 \Delta R$. If $\Delta R =$ a few R_S , and $\Gamma \sim 15$, then $R_{\text{diss}} \sim 10^3 R_S$. Larger val-

ues are possible for larger Γ or for larger ΔR . Alternatively, R_{diss} may be set by the pressure balance between the jet and the external medium. In this case R_{diss} is larger for a larger jet pressure, and then for a larger jet power.

ACKNOWLEDGMENTS

FT and GB acknowledge financial contribution from a PRIN–INAF–2011 grant. We acknowledge the use of public data from the *Swift* data archive. This research made use of the NASA/IPAC Extragalactic Database (NED) which is operated by the Jet Propulsion Laboratory, Caltech, under contract with the NASA, and of data obtained from the High Energy Science Archive Research Center (HEASARC), provided by NASA’s GSFC, and of the XRT Data Analysis Software (XRTDAS) developed under the responsibility of the ASI Science Data Center (ASDC), Italy.

REFERENCES

- Abdo A.A. et al., 2009, *ApJ*, 700, 597
 Abdo A.A. et al., 2010, *ApJ*, 715, 429
 Blazejowski M., Sikora M., Moderski R. & Madejski G.M., 2000, *ApJ*, 545, 107
 Bloom S.D. et al., 1997, *ApJ*, 490, L145
 Breeveld A.A. et al., 2010, *MNRAS*, 406, 1687
 Calderone G., Ghisellini G., Colpi M. & Dotti M., 2013, *MNRAS*, in press (astro-ph/1212.1181)
 Cardelli J.A., Clayton G.C. & Mathis J.S., 1989, *ApJ*, 345, 245
 Carrasco L., Recillas E., Mayya D.Y. & Carraminana A., 2013, *ATel* 4736
 Dermer C.D. & Schlickeiser R., 1993, *ApJ*, 416, 458
 Donato D., Cheung C.C. & Tanaka Y., 2013, *ATel* 4742
 Foschini L., Ghisellini G., Tavecchio F., Bonnoli G. & Stamerra A., 2011, *Fermi Symposium proceedings eConf C110509* (astro-ph/1110.4471)
 Francis P.J., Hewett P.C., Foltz C.B., Chaffee F.H., Weymann R.J., Morris S.L., 1991, *ApJ*, 373, 465
 Ghisellini G. & Tavecchio F., 2009, *MNRAS*, 397, 985
 Ghisellini G., Maraschi L. & Tavecchio F., 2009, *MNRAS*, 396, L105
 Ghisellini G., Tavecchio F., Foschini L., Ghirlanda G., Maraschi L. & Celotti A., 2010, *MNRAS*, 402, 497
 Ghisellini G., Tavecchio F., Foschini L., Sbarrato T., Ghirlanda G. & Maraschi L., 2012, *MNRAS*, 425, 1371
 Healey S.E. et al., 2008, *ApJS*, 175, 97
 Kalberla P.M.W., Burton W.B., Hartmann D., Arnal E.M., Bajaja E., Morras R. & Pöppel W.G.L. 2005, *A&A*, 440, 775
 Mattox J.R. et al., 1996, *ApJ*, 461, 396
 Nolan P.L. et al. 2012, *ApJS*, 199, 31
 Padovani P., Giommi P. & Rau A., 2012, *MNRAS*, 422, L48
 Padovani P. & Giommi P., 1995, *ApJ*, 444, 567
 Pian E. et al., 1998, *ApJ*, 492, L17
 Poole T.S. et al., 2008, *MNRAS*, 383, 627
 Shakura N.I. & Syunayev R.A., 1973, *A&A*, 24, 337
 Shaw M.S., Romani R.W., Healey S.E., Cotter G., Michelson P.F. & Readhead A.C.S., 2009, *ApJ*, 704, 477
 Sikora M., Begelman M.C. & Rees M.J., 1994, *ApJ*, 421, 153
 Sikora M., Blazejowski M., Moderski R., Madejski G.M., 2002, *ApJ*, 577, 78
 Tagliaferri G. et al., 2000, *A&A*, 354, 431
 Tanaka Y., 2013, *ATel* 4735
 Tanaka Y.T. et al., 2011, *ApJ*, 733, 19
 Tavecchio F., & Ghisellini G., 2008, *MNRAS*, 386, 945
 Tavecchio F. et al., 2001, *ApJ*, 554, 725
 Vanden Berk D.E. et al., 2001, *AJ*, 122, 549